

# Dynamics and correlation length scales of a glass-forming liquid in quiescent and sheared conditions

Wen-Sheng Xu, Zhao-Yan Sun\*, and Li-Jia An†

*State Key Laboratory of Polymer Physics and Chemistry, Changchun Institute of Applied Chemistry, Chinese Academy of Sciences, Changchun 130022, People's Republic of China*

(Dated: November 26, 2018)

We numerically study dynamics and correlation length scales of a colloidal liquid in both quiescent and sheared conditions to further understand the origin of slow dynamics and dynamic heterogeneity in glass-forming systems. The simulation is performed in a weakly frustrated two-dimensional liquid, where locally preferred order is allowed to develop with increasing density. The four-point density correlations and bond-orientation correlations, which have been frequently used to capture dynamic and static length scales  $\xi$  in a quiescent condition, can be readily extended to a system under steady shear in this case. In the absence of shear, we confirmed the previous findings that the dynamic slowing down accompanies the development of dynamic heterogeneity. The dynamic and static length scales increase with  $\alpha$ -relaxation time  $\tau_\alpha$  as power-law  $\xi \sim \tau_\alpha^\mu$  with  $\mu > 0$ . In the presence of shear, both viscosity and  $\tau_\alpha$  have power-law dependence on shear rate in the marked shear thinning regime. However, dependence of correlation lengths cannot be described by power laws in the same regime. Furthermore, the relation  $\xi \sim \tau_\alpha^\mu$  between length scales and dynamics holds for not too strong shear where thermal fluctuations and external forces are both important in determining the properties of dense liquids. Thus, our results demonstrate a link between slow dynamics and structure in glass-forming liquids even under nonequilibrium conditions.

PACS numbers: 61.20.Ja, 61.20.Lc, 64.70.P-

## I. INTRODUCTION

Glass can be formed in a variety of molecular and colloidal systems, but the nature of the glass transition remains elusive despite intensive research [1–4]. It is commonly observed that time scales, such as structural relaxation time, dramatically increase on the approach to the glass transition point with little change in the static structure of the liquid. This is the reason why the research on the glass transition for a long time has been focused on time scales much more than length scales. In the past decade, however, both experiments and simulations have revealed that the relaxation process not only drastically slows down but also becomes progressively more heterogeneous as a liquid approaches its glass transition point [5–11]. The collective nature of the dynamics of the supercooled liquids can indeed date back to the seminal idea of Adam and Gibbs [12] and has been well reviewed in recent publications [4, 13–16]. The phenomenon of growing dynamic heterogeneity approaching the glass transition point also suggests the existence of a growing dynamic length scale in glass-forming systems [9, 11, 17]. As a matter of fact, the issue of characteristic length scales has become one of the main themes of the study on the glass transition [4].

To further understand the origin of the dynamic heterogeneity and explore whether there exist structural signatures connected to the slow dynamics and dynamic

heterogeneity in viscous liquids, several ideas have been put forward. One of the ideas is based on the effect of frustration on crystallization in vitrification. To continuously control frustration, several ways are frequently used in the study [18–20]. One way is to focus on the polydisperse colloidal liquid where frustration can be continuously changed by varying polydispersity [19] (as inspired by the study of crystal nucleation on polydisperse colloids [21]) and another way is to study liquids in negatively curved space where frustration can be controlled by varying space curvature [20] (as motivated from the frustration-based approach of the glass transition [18]). In both cases, if the frustration is not very strong, some local order reminiscent of the crystal structure can develop with increasing density or decreasing temperature. Then, one can readily detect some static correlations (usually by bond-orientation correlation functions) approaching the glass transition and investigate whether these structural signatures are connected to the dynamical properties. Although different interpretations were given for the change of correlation length scales approaching the glass transition point [19, 20], the structural signature of slow dynamics and dynamic heterogeneity does exist at least in these model glass-forming liquids. In particular, a direct relation between dynamic heterogeneity and the so-called medium-range crystalline order (MRCO, i.e., long-lived clusters of particles with high structural order) has been revealed in colloidal dispersions [19]. Another more general method to detect the nontrivial static spatial correlations has been proposed recently, which is motivated from the random first order transition (RFOT) theory [22, 23] (see recent reviews [4, 24] for details on this theory). Within this the-

\*Correspondence author. E-mail: zysun@ciac.jl.cn

†Correspondence author. E-mail: ljan@ciac.jl.cn

ory, the so-called point-to-set correlations [25–29] are believed to capture nontrivial structures of viscous liquids. The idea is to first freeze the position of a set of particles in an equilibrium configuration and then let the system evolve in the presence of the constraint and measure how the position of the remaining particles is affected. Thus, the point-to-set length is a measure of the spatial extent over which the effect of equilibrium amorphous boundary conditions propagates. Numerical simulations have confirmed qualitatively the growth of the point-to-set correlations [25] and its connection to the dynamic correlations has also been explored recently [26, 27]. Besides, the structural features of slow dynamics in viscous liquids have also been investigated in Refs. [30–36].

In recent years, the study of supercooled liquids and glasses under nonequilibrium conditions (e.g., under shear) has also attracted considerable attention, with emphasis on their rheological properties and the establishment of the concept of effective temperature [37–41]. The rheology of soft glassy materials not only provide new insight into the nature of the glass transition but also has its own value. One common observation is the marked shear-thinning behavior in glass-forming liquids. In particular, the shear viscosity  $\eta$  is found to decrease with increasing the shear rate  $\dot{\gamma}$  as  $\eta \sim \dot{\gamma}^{-\nu}$  with  $\nu \leq 1$ . Another intriguing finding is that soft glassy materials commonly display the shear banding phenomenon [39], i.e., a system under strong shear spontaneously “phase separates” between a flowing region supporting the shear and an immobile region with no flow. Recently, the question of how dynamic heterogeneity is influenced by the flow has also been addressed [42–48], e.g., numerical simulations [43] revealed the existence of large scale heterogeneities under shear flow and its connection to the non-Newtonian behavior of a supercooled liquid has also been explored, and power-law dependence of the intensity of the dynamic heterogeneity on shear rate has been observed [44–48]. However, it is still not clear how dynamic heterogeneity, MRCO and the associated length scales respond to shear.

In this work, we focus on slow dynamics and dynamic heterogeneity of a colloidal glass-forming liquid and their structural features in both quiescent and sheared conditions. We use a weakly frustrated two-dimensional (2D) liquid as our model system, where crystallization can be avoided and locally preferred order is allowed to develop with increasing density. The four-point density correlations and bond-orientation correlations, which have been frequently used to capture the dynamic and static length scales  $\xi$  in a quiescent condition, can be readily extended to a system under steady shear in this case. We confirmed the previous findings in the absence of shear that slow dynamics accompanies the development of dynamic heterogeneity. Both dynamic and static length scales increase with  $\alpha$ -relaxation time  $\tau_\alpha$  as power-law  $\xi \sim \tau_\alpha^\mu$  with  $\mu > 0$ . In the presence of shear, both  $\eta$  and  $\tau_\alpha$  have power-law dependence on  $\dot{\gamma}$  in the marked shear thinning regime. However, dependence of the dynamic and static correlation lengths on  $\dot{\gamma}$  cannot be described by power

laws in the same regime. We further find that the relation  $\xi \sim \tau_\alpha^\mu$  between length scales and dynamics holds for not too strong shear where thermal fluctuations and applied forces are both important in determining the properties of dense liquids. The paper is organized as follows: In Sec. II, we show the model and methods used in this study, and then we present results and discuss structural signatures of slow dynamics and dynamic heterogeneity in the absence of shear in Sec. III. Results under steady shear are given in Sec. IV. Finally, Sec. V summarizes our results.

## II. MODEL AND METHODS

The model we focus here is a 2D liquid, in which the particles interact via the Weeks-Chandler-Andersen (WCA) potential [49]:

$$U_{jk}(r) = \begin{cases} 4\epsilon[(\sigma_{jk}/r)^{12} - (\sigma_{jk}/r)^6 + 1/4], & \text{for } r < 2^{1/6}\sigma_{jk} \\ 0, & \text{otherwise,} \end{cases} \quad (1)$$

where  $\epsilon$  is the depth of the potential well,  $r$  is the distance between two particles, and  $\sigma_{jk} = (\sigma_j + \sigma_k)/2$  with  $\sigma_j$  the diameter of particle  $j$ . As the WCA potential is short-ranged repulsive, a WCA liquid at low temperatures behaves as a colloidal liquid. Although recent simulations [50, 51] have shown that the longer-ranged attractive interactions can affect the dynamics of viscous liquids in quantitatively and qualitatively ways, we expect that the conclusions in our work will not be changed since the purely repulsive model can also capture the essential features of a typical glass-forming liquid. To introduce weak frustration on crystallization in vitrification, the particle diameters were chosen equidistantly from the range 0.8 – 1.2 with an interval of 0.01, then the polydispersity for the system is  $\Delta = \sqrt{\langle \sigma^2 \rangle - \langle \sigma \rangle^2} / \langle \sigma \rangle = 11.98\%$ , where  $\langle x \rangle$  is the average of variable  $x_j$  among all the particles. Such polydispersity can avoid crystallization in the system and allow static structural order to develop with increasing density. In principle, Brownian dynamics simulation is a more faithful method to study colloids. However, previous work has suggested that at long times, when particles have collided many times, Brownian and Newtonian systems show qualitatively the same phenomenology [52]. We employed molecular dynamics simulation in the  $NVT$  ensemble, where Newton’s equations of motion were integrated for  $N = 1000$  particles with the velocity form of the Verlet algorithm under periodic boundary conditions and the temperature  $T$  was maintained by the Nosé-Hoover thermostat [53]. All the particles have the same mass  $m$ . Length and time were expressed in units of  $\langle \sigma \rangle$  and  $\sqrt{m \langle \sigma \rangle^2 / \epsilon}$ . The time step is  $\Delta t = 0.002$ . For convenience, the temperature  $T$  in our simulation is fixed at  $k_B T / \epsilon = 0.025$  with  $k_B$  the Boltzmann’s constant. We use the area fraction  $\phi = (1/V) \times \sum_{j=1}^N \pi(\sigma_j/2)^2$  ( $V = L^2$  with  $L$  the box dimension) as a control parameter. In this work, we did

not make a correction to the softness of the WCA potential and map a WCA system to a hard-sphere system by using the effective diameter since we only want to focus the glassy behavior as the density varies. In athermal colloids,  $1/\phi$  plays the same role as temperature in molecular liquids. The area fraction  $\phi$  in this work covers the range from 0.62 to 0.65 ( $L = 35.01 \sim 35.85$ ). In order to check the possible finite size effects, we also performed simulations for a system with  $N = 4000$  in the absence of shear, and we found the qualitative agreement with the results from the smaller system. Thus, we only show the results with  $N = 1000$  in this paper. At each  $\phi$ , the system was equilibrated for  $5 \times 10^7$  time steps first before collecting data and 8 independent runs were performed.

In order to study the system under steady shear, we used the nonequilibrium molecular dynamics (NEMD) SLLOD algorithm [54, 55]. The SLLOD equations of motion are given by:

$$\begin{aligned} \frac{d\mathbf{r}_j}{dt} &= \frac{\mathbf{p}_j}{m} + \mathbf{r}_j \cdot \nabla \mathbf{v}, \\ \frac{d\mathbf{p}_j}{dt} &= - \sum_{j \neq k} \frac{\partial U(\mathbf{r}_{jk})}{\partial \mathbf{r}_{jk}} - \mathbf{p}_j \cdot \nabla \mathbf{v}, \end{aligned} \quad (2)$$

where  $\mathbf{p}_j$  and  $\mathbf{r}_j$  are the peculiar momentum and laboratory position of particle  $j$ , and  $\nabla \mathbf{v}$  is the gradient of the streaming velocity  $\mathbf{v}$ . Combining with the Lees-Edwards boundary conditions [56], these equations of motion can generate homogeneous flow, which means that no instability such as shear banding [39] occurs in our simulations. In the case of planar Couette shear flow,  $\mathbf{v}$  has only one non-zero component, which is given by  $\dot{\gamma}y\hat{\mathbf{x}}$ , where  $\dot{\gamma}$  is the shear rate and  $\hat{\mathbf{x}}$  the unit vector along the  $x$  axis. Here the velocity gradient is in the  $y$  direction, and the streaming velocity in the  $x$  direction. The shear rate  $\dot{\gamma}$  varies from  $10^{-6}$  to 0.03, covering the linear and nonlinear response regimes of rheology. For each state point under shear, 16 independent runs were performed to improve the statistics.

### III. SLOW DYNAMICS AND GROWING LENGTH SCALES AT EQUILIBRIUM

In this section, we first describe slow dynamics and growing dynamic heterogeneity approaching the glass transition point in a quiescent condition, and then discuss growing dynamic and static length scales and structural features of the slow dynamics. Relation between structure and dynamics in polydisperse colloidal liquids has also been discussed recently in Refs. [19] and the emergence of long-lived clusters of particles with higher order can be connected to slow dynamics and dynamic heterogeneity. Structural features of slow dynamics and dynamic heterogeneity are also confirmed by our results.

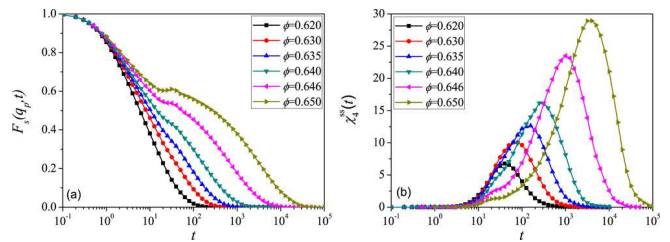


FIG. 1: The self part of (a) the intermediate scattering function  $F_s(q_p, t)$  and (b) the four-point susceptibility  $\chi_4^{ss}(t)$  at representative area fractions.

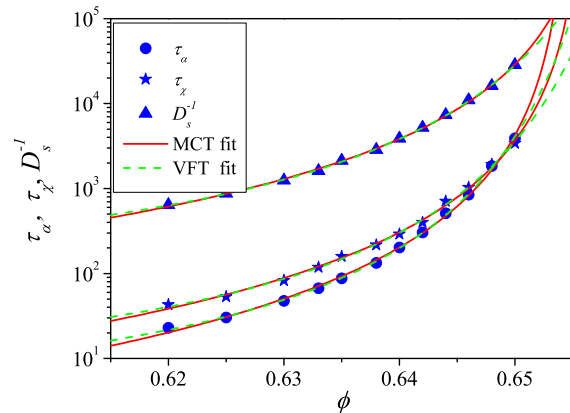


FIG. 2:  $\phi$ -dependence of  $\alpha$ -relaxation time  $\tau_\alpha$ , peak time of the four-point susceptibility  $\tau_\chi$  and self-diffusion constant  $D_s$ . The red solid lines are the results of the power-law fittings  $\tau_\alpha \sim (\phi_c - \phi)^{-\gamma}$  with  $\gamma = 2.7$  for  $\tau_\alpha$ ,  $\gamma = 2.6$  for  $\tau_\chi$  and  $\gamma = 2.4$  for  $D_s^{-1}$ . Excellent fits are obtained to all data for a single value  $\phi_c = 0.656 \pm 0.001$ . The green dashed lines are the results of the Vogel-Fulcher-Tamman fittings  $\tau_\alpha \sim \exp[D\phi/(\phi_0 - \phi)]$  with  $D = 0.22$  for  $\tau_\alpha$ ,  $D = 0.23$  for  $\tau_\chi$  and  $D = 0.25$  for  $D_s^{-1}$ . Excellent fits are obtained to all data for a single value  $\phi_0 = 0.671 \pm 0.004$ .

#### A. Slow dynamics and growing dynamic heterogeneity approaching the glass transition

We first consider the  $\phi$  dependence of the potential energy  $E_p$  and the pressure  $p$  of the system. We find that both  $E_p$  and  $p$  are smooth functions of  $\phi$  (data not shown), indicating that crystallization indeed does not occur. Further confirmations for the avoidance of crystallization come from the positional order and the spatial correlation of hexatic order, which will be shown later.

The dynamic slowing down can be characterized by calculating the self part of the intermediate scattering function (ISF):

$$F_s(q_p, t) = \frac{1}{N} \left\langle \sum_{j=1}^N \exp\{i\mathbf{q}_p \cdot [\mathbf{r}_j(t) - \mathbf{r}_j(0)]\} \right\rangle, \quad (3)$$

where  $\langle \dots \rangle$  indicates the thermal average,  $i = \sqrt{-1}$

and the wave number  $q_p$  corresponds to the first peak of the static structure factor (which will be shown later).  $F_s(q_p, t)$  can reflect structural relaxation process of a liquid and representative results for several area fractions are shown in Fig. 1(a). We observe that the relaxation slows down and becomes more stretched as  $\phi$  increases. In particular, a two-step decay emerges at high enough area fractions, reflecting the rattling motion of particles trapping within cages at short times ( $\beta$ -relaxation) and the motion of particles escaping from the cages at long times ( $\alpha$ -relaxation). We define  $\alpha$ -relaxation time as  $F_s(q_p, t = \tau_\alpha) = 0.2$  (we have checked that choosing other values will not alter the qualitative results), which is plotted as a function of  $\phi$  in Fig. 2. Clearly,  $\tau_\alpha$  drastically increase as  $\phi$  increases. For the density range investigated,  $\tau_\alpha$  can be well fitted by the mode-coupling-theory (MCT) power-law [57]:  $\tau_\alpha \sim (\phi_c - \phi)^{-\gamma}$ , where  $\phi_c$  is the MCT glass transition point, or the Vogel-Fulcher-Tamman (VFT) law:  $\tau_\alpha \sim \exp[D\phi/(\phi_0 - \phi)]$ , where  $D$  is the fragility index and  $\phi_0$  is the ideal glass-transition point.

For the glass-forming liquids, the dynamic slowing down accompanies growing dynamic heterogeneity. We quantify the dynamic heterogeneity by the self part of the four-point density correlations [9], which dominates results of the total four-point density correlations [9, 17]. A time-dependent self-overlap order parameter  $Q_s(t)$  is defined as

$$Q_s(t) = \frac{1}{N} \left\langle \sum_{j=1}^N w(|\mathbf{r}_j(t) - \mathbf{r}_j(0)|) \right\rangle, \quad (4)$$

with  $w = 1(0)$  for  $|\mathbf{r}_j(t) - \mathbf{r}_j(0)| \leq (>)0.4 < \sigma >$ . The threshold 0.4 was determined by considering the peak height of the four-point susceptibility  $\chi_4^{ss}(t) = \frac{1}{N^2} [\langle Q_s(t)^2 \rangle - \langle Q_s(t) \rangle^2]$  becoming maximal for  $\phi = 0.64$ .  $\chi_4^{ss}(t)$  measures the extent to which the dynamics at any two points in space are correlated within a time interval. Typical results for  $\chi_4^{ss}(t)$  are shown in Fig. 1(b). As can be seen, the peak height of  $\chi_4^{ss}(t)$  increases and the peak time  $\tau_\chi$  shifts to larger times as  $\phi$  increases, which indicates that the dynamics not only slows down but also becomes progressively more heterogeneous on the approach to the glass transition.  $\tau_\chi$  can also be well fitted by MCT power-law or VFT law, as shown in Fig. 2. We also present  $\phi$  dependence of the self-diffusion constant  $D_s$  in Fig. 2, as evaluated by using Einstein relation from the long-time data of the mean squared displacements. Independent fits give these three types of data with single parameters  $\phi_c = 0.656 \pm 0.001$  and  $\phi_0 = 0.671 \pm 0.004$ .

As mentioned in Sec. I, the development of dynamic heterogeneity suggests the existence of a growing dynamic length scale, which can be investigated by the four-point, time-dependent structure factor for the self-overlapping particles, which is defined as

$$S_4^{ss}(q, t) = \frac{L^2}{N^2} \langle \tilde{\rho}(q, t) \tilde{\rho}(-q, t) \rangle, \quad (5)$$

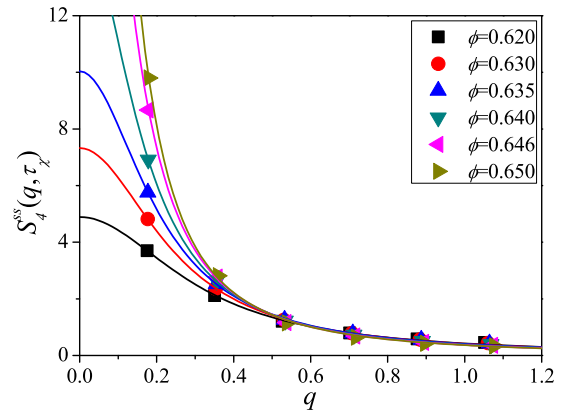


FIG. 3: The structure factor of the self-overlapping particles  $S_4^{ss}(q, t)$  at low- $q$  region for several area fractions. The solid lines are the results of the OZ fittings (see text).

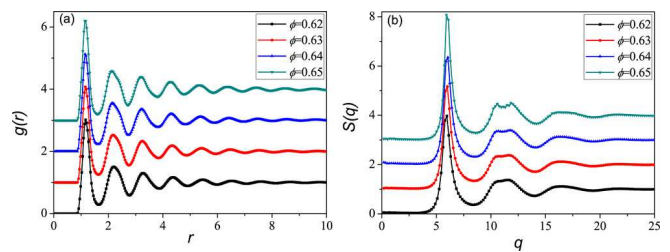


FIG. 4: (a) The pair correlation function  $g(r)$  and (b) the static structure factor  $S(q)$  at low- $q$  region at varying  $\phi$ . The results have been shifted for clarity.

where  $\tilde{\rho}(q, t) = \sum_{j=1}^N w(|\mathbf{r}_j(t) - \mathbf{r}_j(0)|) \exp[i\mathbf{q} \cdot \mathbf{r}_j(0)]$ . Here, the time  $t$  is often taken as  $\tau_\chi$ , where dynamic heterogeneity becomes most pronounced [9]. Representative results are given in Fig. 3.  $S_4^{ss}(q, \tau_\chi)$  at low- $q$  region can be fitted by the Ornstein-Zernike (OZ) function  $S_0/[1 + (q\xi_4)^2]$  and then we can obtain the dynamic correlation length  $\xi_4$  in this way. We will show the results of  $\xi_4$  later and discuss its link to the slow dynamics.

## B. Growing length scales and structural features of slow dynamics

In Fig. 4, we present results of the pair correlation function  $g(r)$  and the static structure factor  $S(q)$  at varying  $\phi$ , as calculated by  $g(r) = \frac{L^2}{2\pi r \Delta r N(N-1)} \langle \sum_{j \neq k} \delta(r - |\mathbf{r}_{jk}|) \rangle$  and  $S(q) = \frac{1}{N} \langle \rho(q) \rho(-q) \rangle$  respectively, where  $\rho(q) = \sum_{j=1}^N \exp(i\mathbf{q} \cdot \mathbf{r}_j)$ . On one hand, as found in other glass-forming liquids,  $g(r)$  and  $S(q)$  only display slight change on approaching the glass transition (notice that  $\tau_\alpha$  increases by  $\sim 2$  orders of magnitude in the studied density range, as shown in Fig.2). On the other hand, although the long-range positional order is



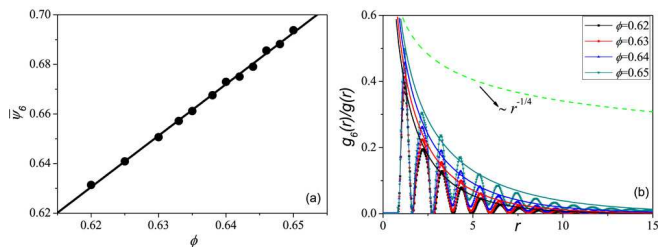


FIG. 5: (a)  $\phi$ -dependence of  $\overline{\Psi}_6$ . The line is a linear fit to the data. (b)  $\phi$ -dependence of  $g_6(r)/g(r)$ . The solid lines are the results of the OZ fittings of the envelopes. The green dashed line is included to stress the fact that crystallization is avoided since  $g_6(r)/g(r)$  decays much faster than  $r^{-1/4}$ . Note that  $g_6(r)/g(r)$  decays as  $r^{-1/4}$  at the boundary between the liquid phase and the hexatic phase [58].

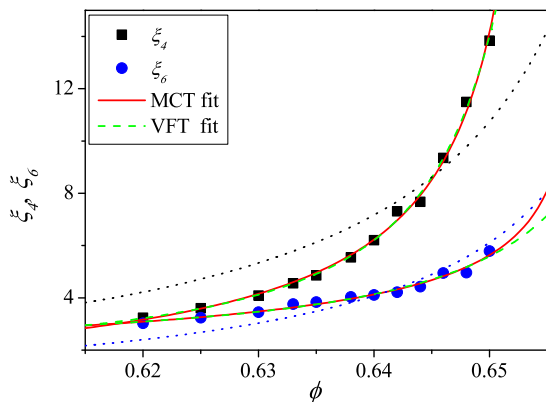


FIG. 6:  $\phi$ -dependence of  $\xi_4$  and  $\xi_6$ . The red solid lines are the results of the MCT fittings  $\sim (\phi_c - \phi)^{-\gamma}$  with  $\phi_c = 0.656$  and  $\gamma = 0.83$  for  $\xi_4$ ,  $\phi_c = 0.658$  and  $\gamma = 0.39$  for  $\xi_6$ . The green dashed lines are the results of the VFT fittings  $\sim \exp[D\phi/(\phi_0 - \phi)]$  with  $\phi_0 = 0.670$  and  $D = 0.074$  for  $\xi_4$ ,  $\phi_0 = 0.678$  and  $D = 0.048$  for  $\xi_6$ . The fitting results of  $\xi_4$  and  $\xi_6$  for  $\phi_c$  and  $\phi_0$  agree well with that of  $\tau_\alpha$ ,  $\tau_\chi$  and  $D_s$  within statistical accuracy. The dotted lines are the fittings of the functional form  $\xi = \xi_0[\phi/(\phi_0 - \phi)]$ .

obviously prevented from Fig. 4, the splitting second peaks in both  $g(r)$  and  $S(q)$  become more apparent as  $\phi$  increases, suggesting the development of the locally preferred order with increasing density.

To characterize the local structure, we used a sixfold bond-orientation order parameter for each particle, which is defined as  $\psi_6^j = \frac{1}{n_j} \sum_{m=1}^{n_j} \exp(i6\theta_m^j)$ . Here,  $n_j$  is the number of the nearest neighbors for particle  $j$  which determined by the Voronoi construction, and  $\theta_m^j$  is the angle between  $(\mathbf{r}_m - \mathbf{r}_j)$  and the  $x$  axis (particle  $m$  is a neighbor of particle  $j$ ). By construction,  $\Psi_6^j = |\psi_6^j|$  is equal to 1 for a perfect hexagonal arrangement of six neighbors around particle  $j$  and 0 for a random arrangement. Then, the time averaged order parameter over  $\tau_\alpha$  for particle  $j$  is

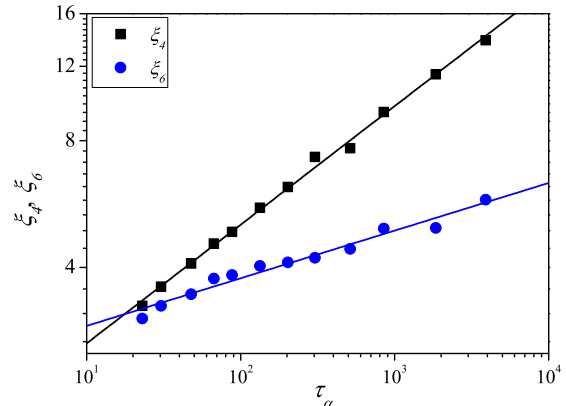


FIG. 7: Log-log plot of  $\xi_4$  and  $\xi_6$  versus  $\tau_\alpha$ . The lines are the results of the power-law ( $\xi \sim \tau_\alpha^\mu$ ) fittings with  $\mu = 0.28$  for  $\xi_4$  and  $\mu = 0.11$  for  $\xi_6$ .

denoted by  $\overline{\Psi}_6^j = \frac{1}{\tau_\alpha} \int_{t_0}^{t_0 + \tau_\alpha} \Psi_6^j dt$ . We also calculated the order parameter of the system  $\overline{\Psi}_6 = \frac{1}{N} \langle \sum_{j=1}^N \Psi_6^j \rangle$ , which is shown in Fig. 5(a) as a function of  $\phi$ . Obviously,  $\overline{\Psi}_6$  monotonically increases in the studied density range as  $\phi$  increases, indicating again the development of the locally preferred order on increasing density. Here we note that hexatic ordering in hard disc systems is a direct consequence of dense packing and manifestation of low configurational entropy, as emphasized in Refs. [19]. The spatial correlation of  $\psi_6^j$  was then calculated as  $g_6(r) = \frac{L^2}{2\pi r \Delta r N(N-1)} \langle \sum_{j \neq k} \delta(r - |\mathbf{r}_{jk}|) \psi_6^j \psi_6^{k*} \rangle$ . The results of  $g_6(r)/g(r)$  for four different area fractions are shown in Fig. 5(b). The envelopes of  $g_6(r)/g(r)$  can be fitted by the OZ function  $r^{-1/2} \exp(-r/\xi_6)$ , and the static correlation length  $\xi_6$  can be obtained in this way. We show results of  $\xi_6$  together with  $\xi_4$  (as estimated from  $S_4^{ss}(q, t)$ ) in Fig. 6. Clearly, they both increase as  $\phi$  increases (or as the dynamics slows down). However, our data cannot be well described by the functional form  $\xi = \xi_0[\phi/(\phi_0 - \phi)]$  (see dotted lines in Fig. 6), which was proposed in Refs. [19]. Instead, they can be well fitted by MCT or VFT functions as shown in Fig. 6, in good agreement with the results of Ref. [9, 17]. In fact, we find that the correlation length scales  $\xi$  have power-law dependence on  $\tau_\alpha$  (i.e.,  $\xi \sim \tau_\alpha^\mu$ ), as evidenced from Fig. 7, where log-log plot of  $\xi_4$  and  $\xi_6$  versus  $\tau_\alpha$  is presented. We will show later that this power-law relation  $\xi \sim \tau_\alpha^\mu$  holds even under shear. Thus, there are indeed structural features of the dynamic slowing down.

To further understand the relation between the slow dynamics and the structure, we also calculated the relaxation of particles with different structural order, as shown in Fig. 8(a). It is observed that the particles with high structural order dominate the relaxation process. Interestingly, the particles with  $\overline{\Psi}_6^j \in (0.2, 0.4)$  relax more

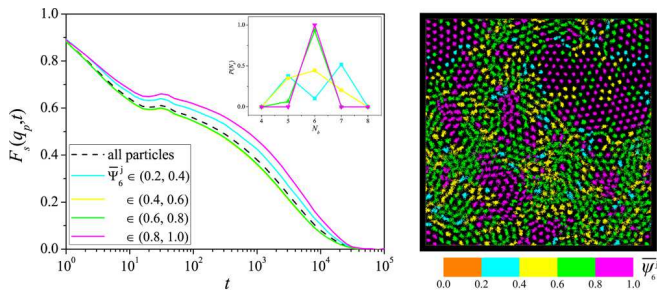


FIG. 8: (Left) Main: The self part of the intermediate scattering function  $F_s(q_p, t)$  for particles with different structural order at  $\phi = 0.65$ . Here,  $\overline{\Psi}_6^j$  is averaged over the time window. Inset: the distribution of neighbors for particles at varying  $\overline{\Psi}_6^j$ . (Right) Corresponding particle trajectory during an interval of  $\tau_\alpha$ . Different colors correspond to different structural order averaged over an interval of  $\tau_\alpha$ . Clearly, particles with the highest structural order (magenta particles) are less mobile than the others and dominate the slow tail of  $F_s(q_p, t)$ .

slowly than those with  $\overline{\Psi}_6^j \in (0.4, 0.8)$ , which is also confirmed by the particle trajectory within a time interval of  $\tau_\alpha$  in Fig. 8(b), i.e., the cyan particles are less mobile than the green and yellow particles, suggesting the existence of an unexpected relationship between hexagonal structure and dynamic heterogeneity. This indicates that particles with specific structures may responsible for the slow relaxation process, which has been pointed out recently in a study of binary soft disks [59]. This feature is also evidenced by the inset of Fig. 8(a) where it reveals that the cyan particles mainly consist of particles with five and seven neighbors.

Therefore, the structural features do exist in our model and the slow dynamics accompanies the development of heterogeneity and growing correlation length scales in the absence of shear. We focus on the correlation between the slow dynamics and the structure under shear flow in the next section.

#### IV. CORRELATION BETWEEN NONEQUILIBRIUM DYNAMICS AND STRUCTURE UNDER SHEAR

When a glass-forming liquid is sheared, marked shear-thinning behavior is expected to appear at sufficiently large shear rates. It is also found in the previous work that the shear viscosity  $\eta$  and  $\tau_\alpha$  change with shear rate  $\dot{\gamma}$  with  $\eta \propto \tau_\alpha \sim \dot{\gamma}^{-\nu}$  ( $\nu > 0$ ). However, it is not clear how correlation lengths vary with  $\dot{\gamma}$  and whether there exists a connection between dynamics and structure in shear flow. In this section, we first investigate the rheological behavior and nonequilibrium dynamics of the system under steady shear and then discuss their structural features.

We first present the time evolution of the sample-averaged shear stress  $\langle \sigma_{xy} \rangle$  after startup shear in Fig.

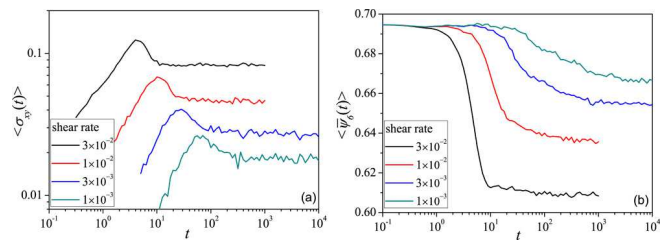


FIG. 9: Time evolution of (a) the shear stress  $\langle \sigma_{xy} \rangle$  and (b) the bond-orientation order parameter  $\overline{\Psi}_6$  after startup shear for several shear rates at  $\phi = 0.65$ . The results are averaged over 200 independent runs.

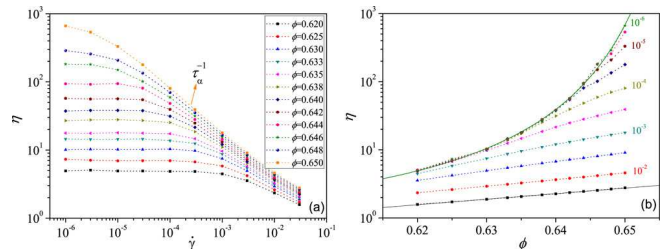


FIG. 10: (a)  $\dot{\gamma}$ -dependence of  $\eta$  at varying  $\phi$ . The arrow indicates that the shear-thinning behavior starts at a shear rate much slower than  $1/\tau_\alpha$  at equilibrium ( $\dot{\gamma} = 0$ ). (b) The same data presented in the form of  $\eta$  versus  $\phi$  at varying  $\dot{\gamma}$ . The solid lines indicate that the weak  $\phi$ -dependence of  $\eta$  at high shear rates crosses over into the strong  $\phi$ -dependence of  $\eta$  (olive line:  $\eta \sim \exp[0.2\phi/(0.667 - \phi)]$ ) at low shear rates.

9(a). Here,  $\sigma_{xy}$  is defined as

$$\sigma_{xy} = \frac{1}{V} \left( \sum_{j=1}^N -\frac{p_{jx}p_{jy}}{m_j} + \sum_{j=1}^N \sum_{j>k} r_{jkx} \frac{\partial U(\mathbf{r}_{jk})}{\partial r_{jky}} \right). \quad (6)$$

It is seen that the system reaches the steady state after a transient period (typically, it needs to be significantly larger than  $\dot{\gamma}^{-1}$ ). Before entering the steady state, a peak emerges at some yielding shear stress. This phenomenon is usually called overshoot behavior (or yielding behavior). Although it was commonly found in many systems [43, 60, 61], its detailed mechanism remains elusive. Here we show in Fig. 9(b) that overshoot behavior also accompanies structural change in our system. The viscosity of the system was then calculated from the steady state shear stress by using the constitutive equation  $\eta = \sigma_{xy}/\dot{\gamma}$ . The shear rate dependence of  $\eta$  is given in Fig. 10(a). The same data are also represented in the alternative form of  $\eta$  versus  $\phi$  in Fig. 10(b). Clearly, the rheological behavior becomes Newtonian at low shear rates where  $\eta$  approached its equilibrium value ( $\dot{\gamma} = 0$ ), and non-Newtonian at high shear rates where marked shear thinning ( $\eta \sim \dot{\gamma}^{-\nu}$ ) behavior displays. It should be noted that the shear-thinning behavior starts at a shear rate much smaller than the inverse of  $\alpha$ -relaxation time scale at equilibrium, which is consistent with previous results [11, 43] and indicates that there may be a structural

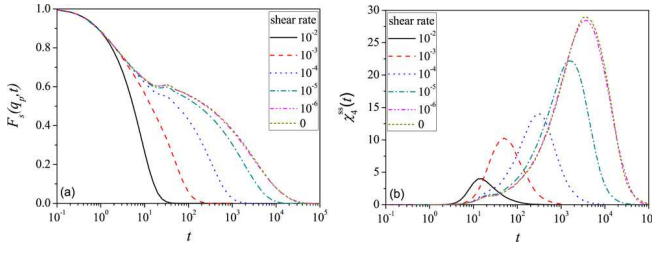


FIG. 11: Shear rate dependence of (a)  $F_s(q_p, t)$  and (b)  $\chi_4^{ss}(t)$  at  $\phi = 0.65$ .

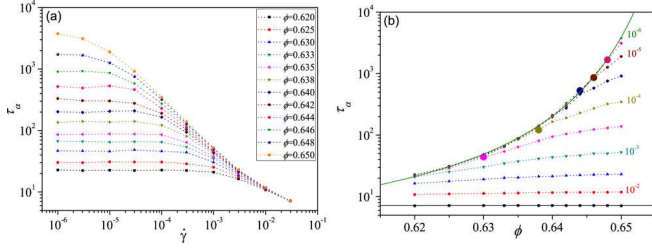


FIG. 12: (a)  $\dot{\gamma}$ -dependence of  $\tau_\alpha$  at varying  $\phi$ . (b) The same data presented in the form of  $\tau_\alpha$  versus  $\phi$  at varying  $\dot{\gamma}$ . The solid lines indicate that the weak  $\phi$ -dependence of  $\tau_\alpha$  at high shear rates crosses over into the strong  $\phi$ -dependence of  $\tau_\alpha$  (olive line:  $\tau_\alpha \sim \exp[0.24\phi/(0.669 - \phi)]$ ) at low shear rates. The larger symbols indicate the crossover area fractions for several shear rates which distinguish equilibrium dynamics from shear-controlled dynamics (see text).

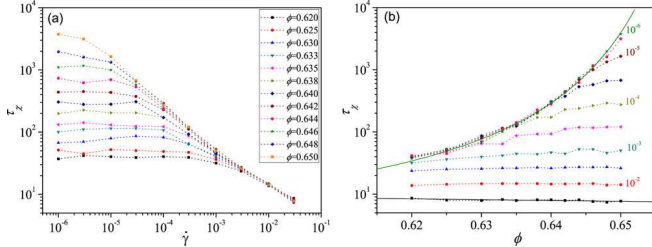


FIG. 13: (a)  $\dot{\gamma}$ -dependence of  $\tau_\chi$  at varying  $\phi$ . (b) The same data presented in the form of  $\tau_\chi$  versus  $\phi$  at varying  $\dot{\gamma}$ . The solid lines indicate that the weak  $\phi$ -dependence of  $\tau_\chi$  at high shear rates crosses over into the strong  $\phi$ -dependence of  $\tau_\chi$  (olive line:  $\tau_\chi \sim \exp[0.25\phi/(0.671 - \phi)]$ ) at low shear rates.

relaxation process much slower than  $\tau_\alpha$  characterizing the decay of the two-body correlation. Meanwhile, we find that  $\eta$  exhibits weak  $\phi$ -dependence at high shear rates and strong  $\phi$ -dependence at low shear rates.

In order to investigate the nonequilibrium dynamics under steady shear, Eqs. (3) and (4) are extended to the system under steady shear, which have the following form:

$$F_s(q, t) = \frac{1}{N} \left\langle \sum_{j=1}^N \exp\{i[(\mathbf{q}_p - \dot{\gamma}tq_{px}\hat{\mathbf{y}}) \cdot \mathbf{r}_j(t) - \mathbf{q}_p \cdot \mathbf{r}_j(0)]\} \right\rangle, \quad (7)$$

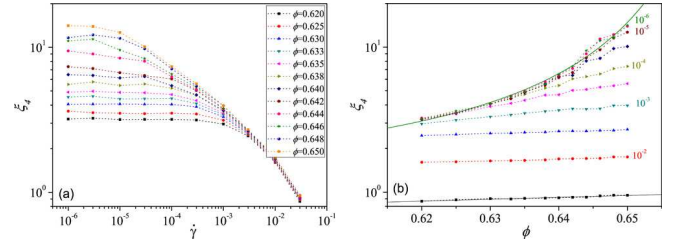


FIG. 14: (a)  $\dot{\gamma}$ -dependence of  $\xi_4$  at varying  $\phi$ . (b) The same data presented in the form of  $\xi_4$  versus  $\phi$  at varying  $\dot{\gamma}$ . The solid lines indicate that the weak  $\phi$ -dependence of  $\xi_4$  at high shear rates crosses over into the strong  $\phi$ -dependence of  $\xi_4$  (olive line:  $\xi_4 \sim \exp[0.11\phi/(0.676 - \phi)]$ ) at low shear rates.

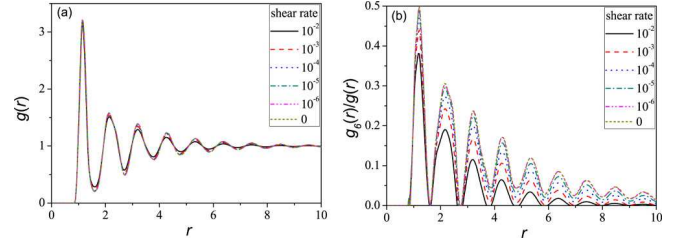


FIG. 15: (a) Shear rate dependence of (a)  $g(r)$  and (b)  $g_6(r)$  at  $\phi = 0.65$ .

and

$$Q_s(t) = \frac{1}{N} \left\langle \sum_{j=1}^N w(|\mathbf{r}_j(t) - \mathbf{r}_j(0) - \dot{\gamma}t\mathbf{y}_j(0)\hat{\mathbf{x}}|) \right\rangle. \quad (8)$$

The results of  $F_s(q_p, t)$  and  $\chi_4^{ss}(t)$  for several shear rates at  $\phi = 0.65$  are given in Fig. 11. Their overall shapes are very similar to those in quiescent conditions and the slow decay of  $F_s(q_p, t)$  satisfies the time-shear superposition property [38]. We present the results of  $\tau_\alpha$  and  $\tau_\chi$  in Figs. 12 and 13. Clearly, they share strong similarities with the viscosity: (1)  $\tau_\alpha \propto \tau_\chi \sim \dot{\gamma}^{-\nu}$  also holds in the marked shear-thinning regime, although the exponent  $\nu$  is different for  $\eta$ ,  $\tau_\alpha$  and  $\tau_\chi$ ; (2)  $\eta$ ,  $\tau_\alpha$  and  $\tau_\chi$  all exhibit weak  $\phi$ -dependence at high  $\dot{\gamma}$  and strong  $\phi$  dependence at low  $\dot{\gamma}$ ; (3) for sufficiently low  $\dot{\gamma}$ , there exists a crossover area fraction  $\phi(\dot{\gamma})$  distinguishing equilibrium dynamics from shear-controlled dynamics (see larger symbols in Fig. 12(b)). Specifically,  $\eta$ ,  $\tau_\alpha$  and  $\tau_\chi$  are nearly independent on shear rate below  $\phi(\dot{\gamma})$  and strongly affected by both  $\phi$  and  $\dot{\gamma}$  above  $\phi(\dot{\gamma})$ . This phenomenon is in good agreement with findings of Ref. [62].

We can also obtain a dynamic correlation length  $\xi_4$  from the four-point structure factor (Eq. (5)) [63], which is shown in Fig. 14.  $\xi_4$  also decreases in the marked shear thinning regime as  $\dot{\gamma}$  increases. However, contrary to the previous study [44–48], we find that power laws fail to describe its dependence on  $\dot{\gamma}$  even in the marked shear thinning regime.

Turing to the static properties, we present the shear rate dependence of  $g(r)$  and  $g_6(r)$  in Fig. 15. We find

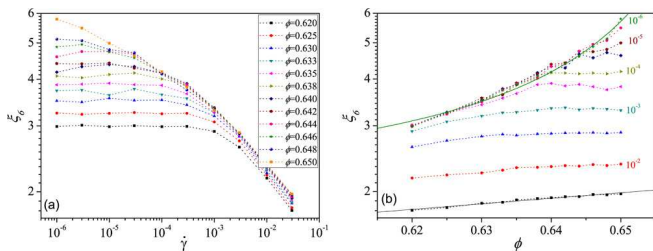


FIG. 16: (a)  $\dot{\gamma}$ -dependence of  $\xi_6$  at varying  $\phi$ . (b) The same data presented in the form of  $\xi_6$  versus  $\phi$  at varying  $\dot{\gamma}$ . The solid lines indicate that the weak  $\phi$ -dependence of  $\xi_6$  at high shear rates crosses into the strong  $\phi$ -dependence of  $\xi_6$  (olive line:  $\xi_6 \sim \exp[0.05\phi/(0.678 - \phi)]$ ) at low shear rates.

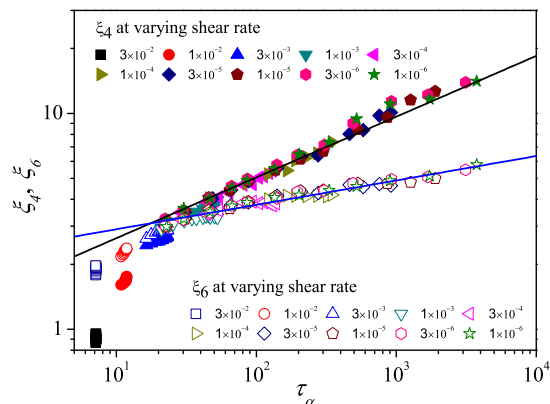


FIG. 17: Log-log plot of  $\xi_4$  and  $\xi_6$  versus  $\tau_\alpha$  at varying  $\dot{\gamma}$ . The lines are the same as those in Fig. 7.

that only weak changes display in the radial distribution function (Fig. 15(a)), while pronounced changes are observed in the bond-orientation correlation function (Fig. 15(b)).  $g_6(r)/g(r)$  under shear can also be well fitted by the OZ function and then we can calculate the static correlation length  $\xi_6$  under shear, which is shown in Fig. 16. Clearly, power laws also fail to describe  $\dot{\gamma}$  dependence of  $\xi_6$ . We also confirm that  $\xi_4$  and  $\xi_6$  under shear have similar dependence on  $\dot{\gamma}$  although we didn't find an empirical or theoretical functional form for them. However, their connection to slow dynamics under steady shear is clear, as evidenced in Fig. 17, where we present log-log plot of  $\xi_4$  and  $\xi_6$  versus  $\tau_\alpha$  at varying  $\dot{\gamma}$ . As can be seen, the power-law relation  $\xi \sim \tau_\alpha^\mu$  only breaks down for very strong shear ( $\dot{\gamma} > \sim 10^{-2}$ ), where externally ap-

plied forces overwhelm random thermal forces and the system exhibit behavior like a normal liquid (e.g., the relaxation process becomes fast and only weak dynamic heterogeneity displays under very strong shear, see Fig. 11). However, the relation  $\xi \sim \tau_\alpha^\mu$  between  $\xi_4$ ,  $\xi_6$  and  $\tau_\alpha$  retains for  $\dot{\gamma} < \sim 10^{-3}$ , where both thermal fluctuations and applied forces are important in determining properties of the liquids and the dynamics slows down and accompanies strong dynamic heterogeneity. Therefore, structure features for the slow dynamics can indeed exist even under shear flow.

## V. CONCLUSIONS

In conclusion, we have investigated structural features of slow dynamics and dynamic heterogeneity in a 2D polydisperse glass-forming liquid in both quiescent and sheared conditions. We have confirmed the previous findings in the absence of shear that slow dynamics accompanies the development of dynamic heterogeneity. The correlation length scales  $\xi$  grow with  $\tau_\alpha$  as a power-law  $\xi \sim \tau_\alpha^\mu$ . In the presence of shear, both  $\eta$  and  $\tau_\alpha$  have power-law dependence on  $\dot{\gamma}$  in the marked shear thinning regime and exhibit weak  $\phi$ -dependence at high shear rates and strong  $\phi$ -dependence at low shear rates. The dynamic and static correlation lengths also decrease with increasing  $\dot{\gamma}$ , but their dependence on  $\dot{\gamma}$  cannot be described by power laws in the same  $\dot{\gamma}$  regime. We further find that the relation  $\xi \sim \tau_\alpha^\mu$  between length scales and dynamics holds for not too strong shear where thermal fluctuations and external forces are both important in determining the properties of dense liquids. Therefore, our results demonstrate a link between slow dynamics and structure in glass-forming liquids even under nonequilibrium conditions and can help to better understand the non-Newtonian behavior of supercooled liquids and glasses.

## Acknowledgments

This work is supported by the National Natural Science Foundation of China (21074137, 50873098, 50930001, 20734003) programs and the fund for Creative Research Groups (50921062). This work is also subsidized by the National Basic Research Program of China (973 Program, 2012CB821500).

- 
- [1] P. W. Andersen, *Science* **267**, 1615 (1995).  
 [2] C. A. Angell, *Science* **267**, 1924 (1995).  
 [3] P. G. Debenedetti and F. H. Stillinger, *Nature (London)* **410**, 259 (2001).  
 [4] L. Berthier and G. Biroli, *Rev. Mod. Phys.* **83**, 587

- (2011).  
 [5] W. K. Kegel and A. van Blaaderen, *Science* **287**, 290 (2000).  
 [6] E. R. Weeks, J. C. Croker, A. C. Levitt, A. B. Schofield, and D. A. Weitz, *Science* **287**, 627 (2000).



- [7] L. Berthier, G. Biroli, J. -P. Bouchaud, L. Cipelletti, D. El Masri, D. L'Hôte, F. Ladieu, and M. Pierno, *Science* **310**, 1797 (2005).
- [8] W. Kob, C. Donati, S. H. Plimpton, P. H. Poole, and S. C. Glotzer, *Phys. Rev. Lett.* **79**, 2827 (1997).
- [9] N. Lačević, F. W. Starr, T. B. Schröder, and S. C. Glotzer, *J. Chem. Phys.* **119**, 7372 (2003).
- [10] R. Yamamoto and A. Onuki, *Phys. Rev. Lett.* **81**, 4915 (1998).
- [11] R. Yamamoto and A. Onuki, *Phys. Rev. E* **58**, 3515 (1998).
- [12] G. Adam and J. H. Gibbs, *J. Chem. Phys.* **43**, 139 (1965).
- [13] M. D. Ediger, *Annu. Rev. Phys. Chem.* **51**, 99 (2000).
- [14] H. C. Andersen, *Proc. Natl. Acad. Sci. U.S.A.* **102**, 6686 (2005).
- [15] L. Berthier, G. Biroli, J. -P. Bouchaud, L. Cipelletti, and W. van Saarloos, Eds., *Dynamical Heterogeneities in Glasses, Colloids and Granular Media* (Oxford University Press, Oxford, 2011).
- [16] L. Berthier, *Physics* **4**, 42 (2011).
- [17] A. S. Keys, A. R. Abate, S. C. Glotzer, and D. J. Durian, *Nature Phys.* **3**, 260 (2007).
- [18] G. Tarjus, S. A. Kivelson, Z. Nussinov, and P. Viot, *J. Phys.: Condens. Matter* **17**, R1143 (2005).
- [19] T. Kawasaki and H. Tanaka, *J. Phys.: Condens. Matter* **23**, 194121 (2011).
- [20] F. Sausset and G. Trajus, *Phys. Rev. Lett.* **104**, 065701 (2010).
- [21] S. Auer and D. Frenkel, *Nature (London)* **413**, 711 (2001).
- [22] T. R. Kirkpatrick and D. Thirumalai, *Phys. Rev. Lett.* **58**, 2091 (1987).
- [23] T. R. Kirkpatrick and P. G. Wolynes, *Phys. Rev. A* **35**, 3072 (1987).
- [24] G. Biroli and J. -P. Bouchaud, arXiv:0912.2542.
- [25] G. Biroli, J. -P. Bouchaud, A. Cavagna, T. S. Grigera and P. Verrocchio, *Nature Phys.* **4**, 771 (2008).
- [26] L. Berthier and W. Kob, *Phys. Rev. E* **85**, 011102 (2012).
- [27] W. Kob, S. Roldan-Vargas and L. Berthier, *Nature Phys.* **8**, 164 (2012).
- [28] C. Cammarota and G. Biroli, arXiv:1106.5513.
- [29] J. -P. Bouchaud and G. Biroli, *J. Chem. Phys.* **121**, 7347 (2004).
- [30] A. Widmer-Cooper, P. Harrowell, and H. Fynewever, *Phys. Rev. Lett.* **93**, 135701 (2004).
- [31] A. Widmer-Cooper and P. Harrowell, *J. Phys.: Condens. Matter* **17**, S4025 (2005).
- [32] A. Widmer-Cooper and P. Harrowell, *Phys. Rev. Lett.* **96**, 185701 (2006).
- [33] A. Widmer-Cooper, H. Perry, P. Harrowell and D. R. Reichman, *Nature Phys.* **4**, 711 (2008).
- [34] J. Mittal, J. R. Errington, and T. M. Truskett, *J. Chem. Phys.* **125**, 076102 (2006).
- [35] U. R. Pedersen, T. B. Schøder, J. D. Dyre, and P. Harrowell, *Phys. Rev. Lett.* **104**, 105701 (2010).
- [36] D. Coslovich and G. Pastore, *J. Chem. Phys.* **127**, 124504 (2007).
- [37] *Jamming and Rheology*, edited by A. J. Liu and S. R. Nagel (Taylor and Francis, New York, 2003).
- [38] L. Berthier and J. -L. Barrat, *J. Chem. Phys.* **116**, 6228 (2002).
- [39] F. Varnik, L. Bocquet, J. -L. Barrat, and L. Berthier, *Phys. Rev. Lett.* **90**, 095702 (2003).
- [40] R. Besseling, E. R. Weeks, A. B. Schofield and W. C. K. Poon, *Phys. Rev. Lett.* **99**, 028301 (2007).
- [41] I. Gazuz, A. M. Puertas, Th. Voigtmann, and M. Fuchs, *Phys. Rev. Lett.* **102**, 248302 (2009).
- [42] J. Goyon, A. Colin, G. Ovarlez, A. Ajdari, and L. Bocquet, *Nature (London)* **454**, 84 (2008).
- [43] A. Furukawa, K. Kim, S. Saito, and H. Tanaka, *Phys. Rev. Lett.* **102**, 016001 (2009).
- [44] C. Heussinger, L. Berthier, and J. -L. Barrat, *Europhys. Lett.* **90**, 20005 (2010).
- [45] C. Heussinger, P. Chaudhuri, and J. -L. Barrat, *Soft matter* **6**, 3050 (2010).
- [46] M. Tsamados, *Eur. Phys. J. E* **32**, 165 (2010).
- [47] K. N. Nordstrom, J. .P. Gollub, and D. J. Durian, *Phys. Rev. E* **84**, 021403 (2011).
- [48] H. Mizuno and R. Yamamoto, *J. Chem. Phys.* **136**, 084505 (2012).
- [49] J. D. Weeks, D. Chandler, and H. C. Andersen, *J. Chem. Phys.* **54**, 5237 (1971).
- [50] L. Berthier and G. Tarjus, *Phys. Rev. Lett.* **103**, 170601 (2009).
- [51] L. Berthier and G. Tarjus, *J. Chem. Phys.* **134**, 214503 (2011).
- [52] H. Löwen, J. -P. Hansen, and J. -N. Roux, *Phys. Rev. A* **44**, 1169 (1991).
- [53] D. Frenkel and B. Smit, *Understanding Molecular Simulation: from Algorithms to Applications* (Academic Press, London, 2002).
- [54] D. J. Evans and G. Morriss, *Statistical Mechanics of Nonequilibrium Liquids* (Cambridge University Press, Cambridge, 2008).
- [55] B. D. Todd and P. J. Daivis, *Mol. Simul.* **33**, 189 (2007).
- [56] M. Allen, *Computer Simulation of Liquids* (Oxford University Press, Oxford, 1987).
- [57] W. Götze, *Complex Dynamics of Glass-Forming Liquids: A Mode-Coupling Theory* (Oxford University Press, Oxford, 2008).
- [58] B. I. Halperin and D. R. Nelson, *Phys. Rev. Lett.* **41**, 121 (1978).
- [59] A. Widmer-Cooper and P. Harrowell, *J. Chem. Phys.* **135**, 224515 (2011).
- [60] P. F. Guan, M. W. Chen, and T. Egami, *Phys. Rev. Lett.* **104**, 205701 (2010).
- [61] X. Li and S. Q. Wang, *Macromolecules* **43**, 5904 (2010).
- [62] L. Angelani, G. Ruocco, F. Sciortino, P. Tartaglia, and F. Zamponi, *Phys. Rev. E* **104**, 061505 (2002).
- [63] Recent simulations [43] indicate that the four-point structure factor  $S_4^{ss}(q, t)$  displays strong anisotropy in the non-Newtonian regime when  $t$  is significantly larger than  $\tau_\chi$ . However, isotropy of  $S_4^{ss}(q, t)$  retains at  $t \leq \tau_\chi$  for both Newtonian and non-Newtonian regime. Thus, we can still calculate  $S_4^{ss}(q, \tau_\chi)$  even in the the non-Newtonian regime and obtain the dynamic correlation length from it.